materials

MDPI

Article

Quantum Confinement Effect in Amorphous In–Ga–Zn–O Heterojunction Channels for Thin-Film Transistors

Daichi Koretomo [1,*], Shuhei Hamada [2], Yusaku Magari [1] and Mamoru Furuta [1,2,3]

1 Engineering Course, Kochi University of Technology, Kami, Kochi 782-8502, Japan; 216007n@gs.kochi-tech.ac.jp (Y.M.); furuta.mamoru@kochi-tech.ac.jp (M.F.)
2 Material Science and Engineering Course, Kochi University of Technology, Kami, Kochi 782-8502, Japan; 225109c@gs.kochi-tech.ac.jp
3 Center for Nanotechnology, Research Institute, Kochi University of Technology, Kami, Kochi 782-8502, Japan
* Correspondence: 216003c@gs.kochi-tech.ac.jp

Received: 12 February 2020; Accepted: 17 April 2020; Published: 20 April 2020

Abstract: Electrical and carrier transport properties in In–Ga–Zn–O thin-film transistors (IGZO TFTs) with a heterojunction channel were investigated. For the heterojunction IGZO channel, a high-In composition IGZO layer (IGZO-high-In) was deposited on a typical compositions IGZO layer (IGZO-111). From the optical properties and photoelectron yield spectroscopy measurements, the heterojunction channel was expected to have the type–II energy band diagram which possesses a conduction band offset (ΔE_c) of ~0.4 eV. A depth profile of background charge density indicated that a steep ΔE_c is formed even in the amorphous IGZO heterojunction interface deposited by sputtering. A field effect mobility (μ_{FE}) of bottom gate structured IGZO TFTs with the heterojunction channel (hetero-IGZO TFTs) improved to ~20 $cm^2\ V^{-1}\ s^{-1}$, although a channel/gate insulator interface was formed by an IGZO–111 (μ_{FE} = ~12 $cm^2\ V^{-1}\ s^{-1}$). Device simulation analysis revealed that the improvement of μ_{FE} in the hetero-IGZO TFTs was originated by a quantum confinement effect for electrons at the heterojunction interface owing to a formation of steep ΔE_c. Thus, we believe that heterojunction IGZO channel is an effective method to improve electrical properties of the TFTs.

Keywords: oxide semiconductor; thin-film transistor; heterojunction; amorphous; device simulation; quantum confinement

1. Introduction

Thin-film transistors (TFTs) based on oxide semiconductors (OSs) have attracted considerable attention for next generation flat-panel displays (FPDs) due to their advantages such as high field effect mobility (μ_{FE}), steep subthreshold swing, and low leakage current [1–9]. Although μ_{FE} of the OS TFTs is more than an order of magnitude higher than that of hydrogenated amorphous silicon (a-Si:H) TFTs, further improvement of the μ_{FE} has been required for OS TFTs to expand their applications [9–13]. Optimization of compositions of the OSs is an approach to improve μ_{FE}, such as an increase of In ratio in the OSs [9,12–15]. However, it was reported the trade-off between μ_{FE} and the reliability of OS TFTs, because an increase of In ratio in the OSs leads to generation defects such as oxygen vacancies [16,17]. As another approach to improve μ_{FE} of the OSs, Koike et al. demonstrated a crystalline ZnO/ZnMgO heterojunction structure that was confirmed to be an improvement of a Hall mobility [18]. Taniguchi et al. reported a heterojunction channel consisting of polycrystalline In–Sn–O on amorphous In–Ga–Zn–O (IGZO) with a type-II energy band lineup, which attributed an improvement of the μ_{FE} to ~20 $cm^2\ V^{-1}\ s^{-1}$ for the TFTs [19].

On the other hand, amorphous OSs have an advantage for the spatial uniformity of their transfer characteristics over a large area; thus, the amorphous OS TFTs are promising candidates for large displays. Various types of heterojunction channels, using amorphous OSs such as IGZO/In–Zn–O (IZO), Hf–In–Zn–O/IZO, Zn–Sn–O/IZO and Al–In–Zn–Sn–O/IZO, have been proposed for TFTs [20–24]. These heterojunction TFTs exhibited excellent μ_{FE} of over 30 cm^2 V^{-1} s^{-1}. The μ_{FE} improvements were mainly induced by the IZO layer, with high-μ_{FE} formed at the channel/gate insulator (GI) interface. Moreover, the heterojunction channels such as IGZO/In–Zn–O/IGZO and In–Ga–Si–O/IGZO/In–Ga–Si–O have also been reported to improve μ_{FE} [25,26]. Thus, the heterojunction channels are considered to be an appropriate approach to boost TFT performances even for amorphous OSs. However, the carrier transport properties in the heterojunction channel have not been discussed in detail, despite a key for the improvement of the μ_{FE} on the amorphous OS TFTs.

We previously reported about the IGZO TFT with a heterojunction channel consisting of different compositions of the amorphous IGZO films. Based on experimental and simulation results obtained by varying a thickness of the barrier layer of the heterojunction channel, it was found that an IGZO heterojunction channel is an effective method to independently improve electrical properties and the reliability of the TFTs [27]. However, the interface properties of the IGZO heterojunction have not been clearly understood. Furthermore, the influence of a conduction band offset (ΔE_c) at the heterojunction interface on the electrical and carrier transport properties has not been analyzed in detail. Thus, it is worth to understand the steepness and ΔE_c at the amorphous IGZO heterojunction interface formed by sputtering.

In this research, the electrical properties of the heterojunction IGZO TFTs were investigated by varying the thickness of a high-In IGZO (IGZO-high-In) well layer, which was deposited on a typical composition of the IGZO (IGZO-111) barrier layer for the heterojunction. In addition, formation of the heterojunction interface was considered from both of the experimental and theoretical results. μ_{FE} of the IGZO TFTs clearly increased, especially in the low gate voltage (V_{GS}) region when the heterojunction channel was formed. From a depth analysis of the background charge density, the transition width at the heterojunction interface was estimated to be less than 3 nm. Device simulation analysis revealed that the ΔE_c, which acts as a potential barrier for electrons, strongly affects carrier transport paths in the heterojunction channel, which leads to an improvement in the μ_{FE} of the TFTs.

2. Experimental Methods

Figure 1a shows a schematic cross-sectional view of the bottom gate structured IGZO TFTs. The IGZO TFTs were fabricated on a heavily doped n-type Si substrate with a 100-nm-thick thermally grown SiO_2. The doped n-type Si substrate and the SiO_2 were used as gate electrode and GI, respectively. The IGZO channels were deposited by radio frequency (RF) magnetron sputtering without intentional substrate heating. As shown in Figure 1b,c, homogeneous channel layers of the 10-nm-thick IGZO-111 (homo-IGZO-111) and the 10-nm-thick IGZO-high-In (homo-IGZO-high-In) were separately prepared for comparison with the heterojunction channel. The oxygen flow ratio (O_2/Ar + O_2) during the depositions were set at 2% and 49% for the IGZO-111 and the IGZO-high-In channels, respectively. Deposition pressure and RF power for both the channels were maintained at 0.5 Pa and 4.4 W cm^{-2}, respectively. For the heterojunction channels as shown in Figure 1d, the IGZO-high-In layer was deposited on the 10-nm-thick-IGZO-111 layer (hetero-IGZO) in a chamber without breaking the vacuum. An upper channel thickness of the IGZO-high-In layer was varied from 2.5 nm to 20 nm, while bottom channel thickness of the IGZO-111 layer was maintained at 10 nm to apply constant electric field at the heterojunction interface. Note here that the deposition conditions for each layer in the heterojunction channel were the same as the homogeneous channels. After formation of the IGZO channel using a shadow mask, a SiO_2 passivation layer (200 nm) was grown by plasma-enhanced chemical vapor deposition at 180 °C using tetraethoxysilane and O_2 as precursors. After opening contact holes by photolithography and dry etching, In–Sn–O source/drain electrodes were deposited

by sputtering through a shadow mask. Finally, the IGZO TFTs were annealed at 350 °C in ambient air for one hour. Channel width and length were 1000 μm and 690 μm, respectively (W/L = 1000/690 μm).

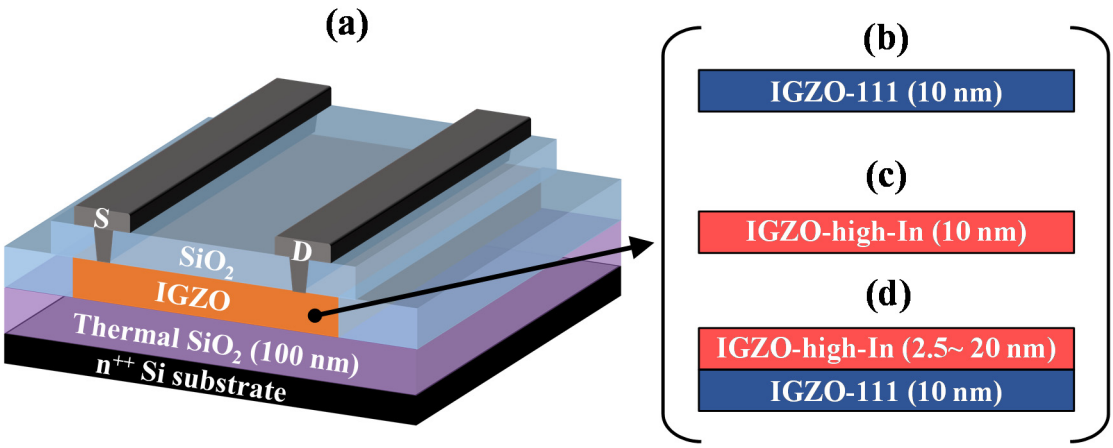

Figure 1. (**a**) Schematic cross-sectional view of the bottom gate structured In–Ga–Zn–O thin-film transistor (IGZO TFT). Channel structures of the (**b**) homogenous typical composition of the IGZO (homo-IGZO-111), (**c**) homogenous high-In IGZO (homo-IGZO-high-In), and (**d**) heterojunction IGZO (hetero-IGZO).

3. Results and Discussion

3.1. Crystallinity of IGZO films

First, the crystallinity of each IGZO layer was evaluated by grazing incidence X-ray diffraction (GIXRD, Rigaku Corp., ATX-G, Tokyo, Japan) using Cu-Kα radiation with the X-ray incident beam angle (ω) of 0.35°. Figure 2 shows GIXRD patterns of the (a) IGZO-111 and (b) IGZO-high-In layers as a function of annealing temperature. Both the IGZO-111 and high-In layer showed crystallization at the annealing temperature of 700–800 °C. The XRD peaks obtained from IGZO-111 after 800 °C attributed to crystalline IGZO, whereas that of IGZO-high-In layer mainly related to crystalline In_2O_3 due to high In ratio in the IGZO [28,29]. On the other hand, both the IGZO-111 and the IGZO-high-In layers retained their amorphous phase at annealing temperatures lower than 600 °C.

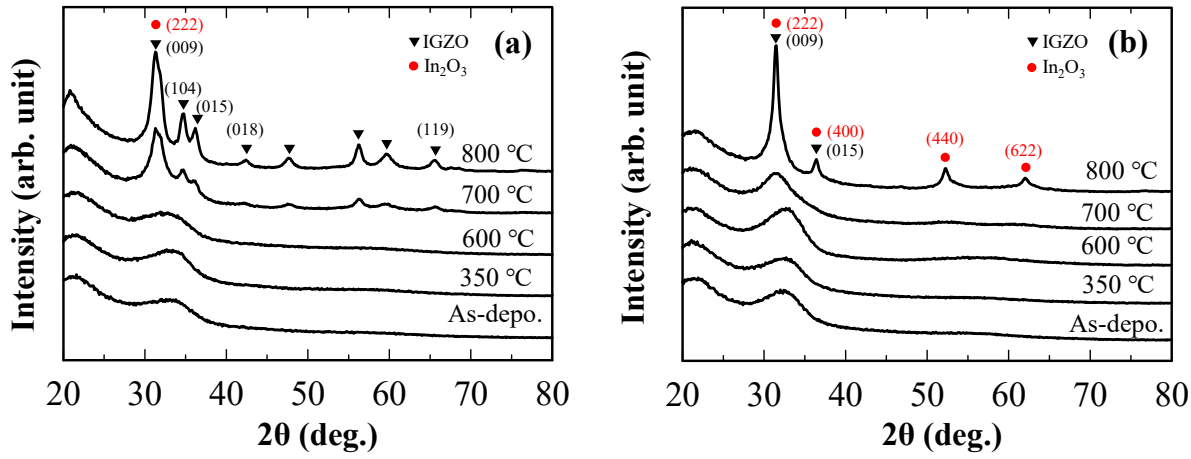

Figure 2. Grazing incidence X-ray diffraction (GIXRD) patterns of (**a**) IGZO-111 and (**b**) IGZO-high-In layers as a function of annealing temperature. Annealing was carried out in air for one hour.

3.2. Band Alignment and Steepness at Heterojunction Interface

Optical band gap (E_g) was estimated by Tauc plot. Valence band maximum (VBM) of the IGZO films was estimated from an ionization potential (I_p), which was measured by photoelectron yield spectroscopy (Bunkoukeiki, BIP-KV202GD, Tokyo, Japan). Figure 3a,b show the Tauc plots and photoemission yield of the IGZO layers. The optical band gaps of the IGZO-111 and the IGZO-high-In layers were estimated to be ~3.1 and ~2.8 eV, respectively. VBMs of the IGZO-111 and the IGZO-high-In layers were ~7.4 and ~7.5 eV, respectively. Since conduction band minimum (CBM) of IGZO mainly consists of In-5s orbitals [30–32], CBM of the IGZO layer would be influence by an In ratio. From these results, the energy band diagram of the IGZO-111 and the IGZO-high-In layers was shown in Figure 3c, suggesting that a ΔE_c of ~0.4 eV might be formed at the heterojunction interface.

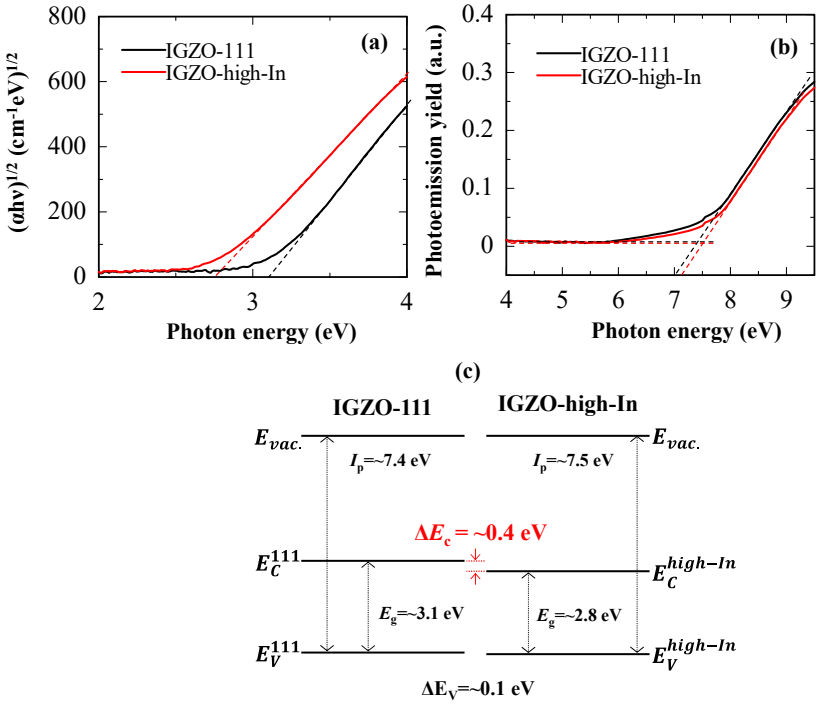

Figure 3. (**a**) Tauc plots and (**b**) photoemission yield of the IGZO-111 and the IGZO-high-In layers after annealing at 350 °C in in ambient air for one hour. (**c**) Energy band diagrams of the IGZO-111 and the IGZO-high-In layers.

To confirm steepness at the heterojunction interface, the depth profile of background charge density (N_{bg}) was evaluated by a Schottky diode (SD) with the heterojunction channel as shown in Figure 4a. Detailed fabrication process of the IGZO SD was reported elsewhere [33]. For the SD with the heterojunction channel, channel thicknesses for the each IGZO layer were set at 30 nm. Carrier density (n_e) of the IGZO-111 was set at ~1×10^{17} cm^{-3} to obtain good Schottky contact, while that of the IGZO-high-In was set at ~3×10^{18} cm^{-3} to enhance the difference of N_{bg} at the heterojunction interface. The N_{bg} was estimated using an equation as shown below [34,35];

$$N_{bg} = \frac{2}{q\varepsilon_0\varepsilon_s}\left[\frac{-1}{\partial\left(1/C_s^2\right)/\partial V}\right] \quad (1)$$

where ε_s and C_s were permittivity and capacitance per unit area of the IGZO, respectively. The C_s was measured using Agilent E4980A LCR meter (California, CA, USA). Figure 4a shows $1/C_s^2$-V characteristic of the Schottky diode at 1 kHz. The $1/C_s^2$ values gradually decreased when the voltage

applied from −1.5 to 0 V. This result indicates that the heterojunction channel was not fully depleted at the negative voltage of −1.5 V. As the voltage exceeded 0 V, the $1/C_s^2$ values decreased steeply.

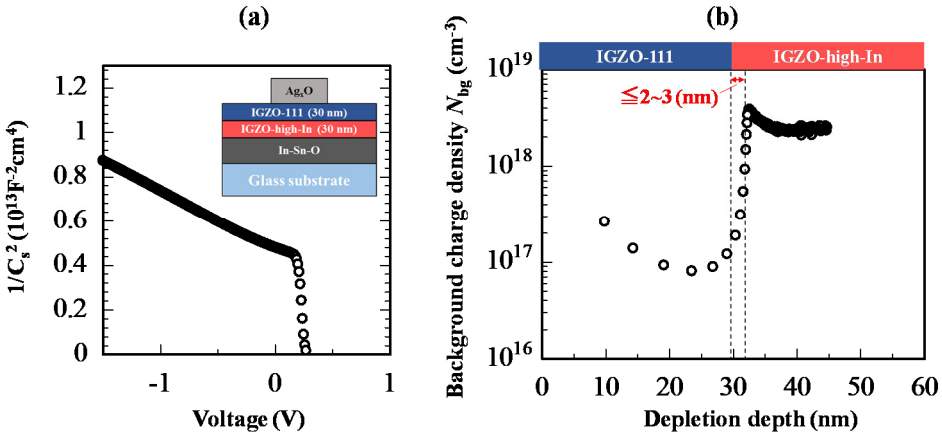

Figure 4. (**a**) $1/C_s^2$-V characteristic of the Schottky diode at 1 kHz. Inset is a schematic cross-sectional view of the Schottky diode with the heterojunction IGZO. The heterojunction IGZO was annealed at 350 °C in ambient air for one hour before deposition of an Ag$_x$O electrode. (**b**) Depth profile of N_{bg} calculated using the $1/C_s^2$-V characteristic. The depth x = 0 nm corresponds to the Ag$_x$O/IGZO-111 interface.

From the $1/C_s^2$-V characteristic, depth profile of N_{bg} in the heterojunction channel was calculated as shown in Figure 4b. The N_{bg} of IGZO-111 layer at the depletion depth from 10 to 30 nm showed approximately 1×10^{17} cm^{-3}, and the N_{bg} of IGZO-high-In steeply increased to ~2×10^{18} cm^{-3} when the depletion depth exceeds 30 nm. The region where the transition of N_{bg} occurred corresponded to the heterojunction interface region. Moreover, the transition width of N_{bg} at the heterojunction interface was estimated to be less than 3 nm. This result indicated that steep ΔE_c would be formed at the heterojunction interface even though both the amorphous IGZO layers were deposited by sputtering.

3.3. TFT Characteristics

Electrical properties of the homogeneous IGZO (homo-IGZO) TFTs were first examined as references for comparison with the heterojunction IGZO (hetero-IGZO) TFTs. Transfer characteristics of the TFTs were measured in dark using precision semiconductor parameter analyzers (Agilent 4156C and 4156A, California, CA, USA). The threshold voltage (V_{th}) was defined as the V_{GS} required to obtain the drain current (I_{DS}) of 1 nA in a linear region. The hysteresis (V_H) was extracted from V_{th} difference between forward and reverse characteristics. The μ_{FE} was calculated from a linear region using the following equation;

$$\mu_{FE} = \frac{g_m}{\frac{W}{L} C_i V_{DS}} \quad (2)$$

where g_m, C_i, and V_{DS} denote transconductance, capacitance of GI per unit area, and drain voltage, respectively.

Figure 5 shows the transfer characteristics of the homo-IGZO-111 and the IGZO-high-In TFTs. Owing to the optimization of a channel thickness and an oxygen flow ratio during the channel deposition [36,37], V_{th} of the homo-IGZO-111 and the IGZO-high-In TFTs were close to zero. From μ_{FE}-V_{GS} curve shown in Figure 5, μ_{FE} of both the homo-IGZO TFTs increased with increasing V_{GS}. The homo-IGZO-high-In TFT exhibited μ_{FE} of 22.9 cm^2 V^{-1} s^{-1}, which is approximately two times higher μ_{FE} than that of the homo-IGZO-111 TFT (12.4 cm^2 V^{-1} s^{-1}). This result indicates that μ_{FE} improvement of the homo-IGZO-high-In TFT was originated by a high-In composition, since large spherical In 5s orbitals mainly form carrier transport paths [26,30,31].

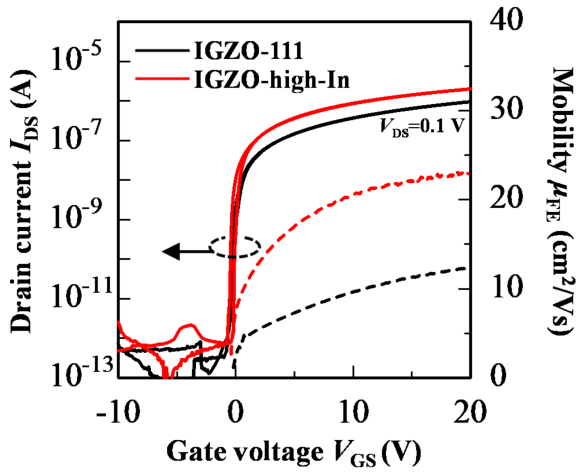

Figure 5. Transfer characteristics of the homo-IGZO-111 and the IGZO-high-In TFTs (V_{DS} = 0.1 V, W/L = 1000/690 μm).

Next, electrical properties of the hetero-IGZO TFTs consisting of the IGZO-high-In on the IGZO-111 were explored. Figure 6 shows the transfer characteristic and μ_{FE}-V_{GS} curves of the hetero-IGZO TFTs with various IGZO-high-In thicknesses. The electrical properties of the hetero-IGZO TFTs summarized in Table 1. The hetero-IGZO TFT with a 2.5-nm-thick upper IGZO-high-In layer showed a μ_{FE} of 9.9 cm^2 V^{-1} s^{-1}, which is almost the same μ_{FE} as homo-IGZO-111 TFT. In contrast, μ_{FE} of the hetero-IGZO TFT significantly improved to 17.2 cm^2 V^{-1} s^{-1} when the upper IGZO-high-In thickness increased from 2.5 to 5.0 nm. The hetero-IGZO TFT with a 10-nm-thick upper IGZO-high-In layer exhibited a μ_{FE} of 19.6 cm^2 V^{-1} s^{-1}. When the upper IGZO-high-In thickness further increased to more than 10 nm, the μ_{FE} saturated to about 21 cm^2 V^{-1} s^{-1}, while V_{th} started to shift in the negative V_{GS} direction. It can be considered that higher negative V_{GS} is required to deplete the channel when the upper IGZO-high-In thickness increase, because the carrier density of the IGZO-high-In layer is higher than that of the IGZO-111 layer. Note here that the μ_{FE} mainly improved in low-V_{GS} region (V_{GS} ≦ 10 V), and it decreased to a similar value as the homo-IGZO-111 TFT at V_{GS} of 20 V. As a result, the μ_{FE}-V_{GS} curves showed a peak at V_{GS} below 10 V. The μ_{FE} improvement would be caused by carrier transport in the high-In layer owing to a formation of steep ΔE_c at the heterojunction interface. To understand an origin of the μ_{FE} improvement in the hetero-IGZO TFTs, carrier transport in the heterojunction channel is discussed based on the results obtained using a device simulation (Atlas, Silvaco Inc., California, CA, USA).

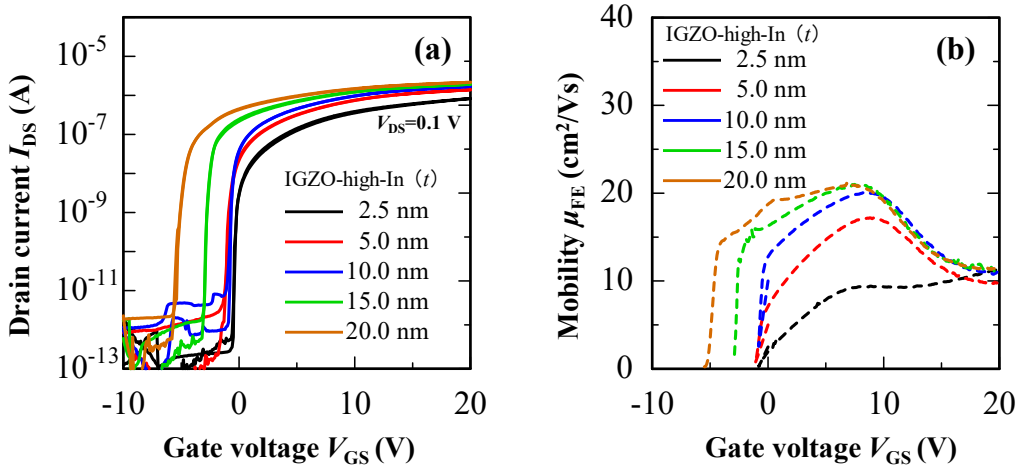

Figure 6. (**a**) Transfer characteristics and (**b**) μ_{FE}-V_{GS} curves of the hetero-IGZO TFTs with various thickness of the IGZO-high-In layer (V_{DS} = 0.1 V, W/L = 1000/690 μm).

Table 1. Summary of electrical properties of the hetero-IGZO TFTs with the various IGZO-high-In thicknesses.

IGZO-High-In Thickness	**2.5 nm**	**5 nm**	**10 nm**	**15 nm**	**20 nm**
IGZO-111 Thickness			**10 nm**		
μ_{FE} (cm^2 V^{-1} s^{-1})	9.9	17.2	19.6	21.8	21.3
S.S. (V/dec.)	0.10	0.10	0.10	0.12	0.15
V_{th} (V)	0	−0.9	−0.9	−3.3	−5.1
V_H (V)	0.0	0.0	0.0	0.0	0.0

Meanwhile, there is no V_H in the hetero-IGZO TFTs, although the homo-IGZO-high-In TFT showed V_H of +1.2 V as shown in Figure 5. These results indicate that the hetero-TFTs showed high μ_{FE} with an improvement of reliability. The reliability results of the IGZO TFTs are discussed in the Figure S1 of Supplementary Information.

3.4. Device Simulation

To understand carrier transport in the hetero-IGZO TFTs, device simulation was carried out using device simulator, Atlas. For the model of IGZO TFTs, a n_e-dependent mobility (μ_d) model with the density of states (DOSs) model was proposed by K. Abe [36]. The n_e-dependent μ_d model is given by the following equations [36];

$$\mu_d = \mu_{d0}(1+\gamma)\left(\frac{n_e}{n_{CR}}\right) \tag{3}$$

$$\gamma = \frac{T_\gamma}{T} + \gamma_0 \tag{4}$$

where μ_{d0} is the intrinsic mobility and n_{CR} is the critical carrier density, and γ is the index parameter.

The simulation parameters, namely, band gap, electron affinity, and n_e dependences of μ_d were defined by the experimental results for both the IGZO layers (see Figure S2, Supplementary Information). The transfer characteristics of the homo-IGZO TFTs shown in Figure 5 were first reproduced to determine the DOSs in each IGZO layer [38–40]. The extracted parameters in both the IGZO models are shown in Table 2. Then, transfer characteristic of the hetero-IGZO TFT with a 10-nm-thick upper high-In layer was reproduced using the same DOSs as homo-IGZO TFTs. Note here that the contacts between S/D electrodes and IGZO back channel were assumed to be ohmic [41].

From above mentioned experimental results, the cause of the μ_{FE} improvement in the hetero-IGZO TFTs is considered to be related to a formation of ΔE_c at the heterojunction interface. To prove the hypothetical origin of the μ_{FE} improvement, influence of the ΔE_c on carrier transport paths of the hetero-IGZO TFT with a 10-nm-thick upper IGZO-high-In layer was analyzed by a device simulation. Figure 7a,b show transfer characteristics and μ_{FE}-V_{GS} curves of the hetero-IGZO TFTs as a function of ΔE_c formed at the heterojunction interface. The drain current and μ_{FE} of the hetero-IGZO TFTs increased with increasing the ΔE_c. When the ΔE_c was set at zero eV, the μ_{FE} of the hetero-IGZO TFT gradually increased with increasing V_{GS} and showed approximately 10 cm^2 V^{-1} s^{-1} at the V_{GS} of 20 V. In contrast, the μ_{FE} in low-V_{GS} region improved when the value of ΔE_c increased. Moreover, the V_{GS} value obtained at maximum μ_{FE} shifted to a positive V_{GS} direction when the ΔE_c increased from 0.1 to 0.45 eV. The experimental μ_{FE}-V_{GS} curve could be reproduced well when the ΔE_c was set at 0.45 eV. Thus, it was confirmed that the ΔE_c at the heterojunction interface strongly influenced μ_{FE} of the hetero-IGZO TFT especially in low-V_{GS} region.

Table 2. Extracted parameters in the homo-IGZO-111 and the IGZO-high-In models.

Symbol	Value (IGZO)		Unit	Description
	−111	-High-In		
N_C	5.0×10^{18}	5.0×10^{18}	cm^{-3}	Effective conduction band density of states
μ_{d0}	14	30	$cm^2\ V^{-1}\ s^{-1}$	Intrinsic electron mobility
n_{CR}	1.0×10^{20}	1.0×10^{20}	cm^{-3}	Critical electron density
T_γ	178.4	178.4	K	γ temperature
γ_0	−0.31	−0.31	—	Gamma at 1/T = 0
W_{ga}	0.7	1.2	eV	Decay energy of acceptor-like Gaussian trap
W_{gd}	0.12	0.12	eV	Decay energy of donor-like Gaussian trap
E_{ga}	0	0	eV	Mean energy of Gaussian acceptor-like trap
E_{gd}	2.6	2.2	eV	Mean energy of Gaussian donor-like trap
N_{ga}	1.5×10^{17}	1.5×10^{17}	$cm^{-3}\ ev^{-1}$	Peak density of Gaussian acceptor-like trap
N_{gd}	1.3×10^{17}	1.3×10^{17}	$cm^{-3}\ ev^{-1}$	Peak density of Gaussian donor-like trap
N_{ta}	1.0×10^{19}	1.0×10^{19}	$cm^{-3}\ ev^{-1}$	Acceptor-like tail trap density
N_{td}	3.0×10^{19}	3.0×10^{19}	$cm^{-3}\ ev^{-1}$	Donor-like tail trap density
W_{ta}	0.01	0.01	eV	Slope of acceptor-like tail trap
W_{td}	0.1	0.1	eV	Slope of donor-like tail trap

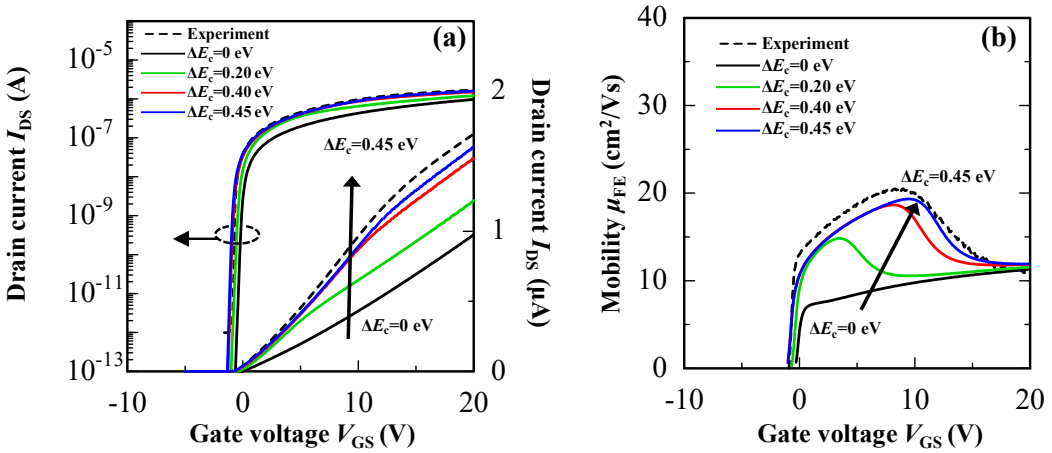

Figure 7. Simulation results of (**a**) transfer characteristics and (**b**) μ_{FE}-V_{GS} curves of the hetero-IGZO TFTs with different ΔE_c. The broken line is an experimental result of the hetero-IGZO TFT.

To clarify influence of the ΔE_c on carrier transport properties, drain current densities in the hetero-IGZO TFTs with different ΔE_c were also analyzed by a device simulation as shown in Figure 8. The drain current densities in the hetero-IGZO TFTs were extracted at the applied V_{GS} of 10 V and V_{DS} of 0.1 V. For the hetero-IGZO TFT with a ΔE_c of zero eV, the drain current densities increased at the IGZO−111/GI interface. Therefore, the hetero-IGZO TFT without ΔE_c exhibited almost the same μ_{FE} as homo-IGZO-111 TFT. On the other hand, the drain current densities at the IGZO-111/GI interface reduced and that at the heterojunction interface increased with increasing the ΔE_c. These results indicate that the carrier transport in the hetero-IGZO-TFTs changed from the IGZO-111/GI interface to the heterojunction interface owing to a quantum confinement effect for electrons when the ΔE_c was formed at the heterojunction interface. Thus, the experimental and device simulation results clarified that the improvement of μ_{FE} in the hetero-IGZO TFTs was mainly caused by a quantum confinement effect for electrons, which was induced by ΔE_c at the heterojunction interface.

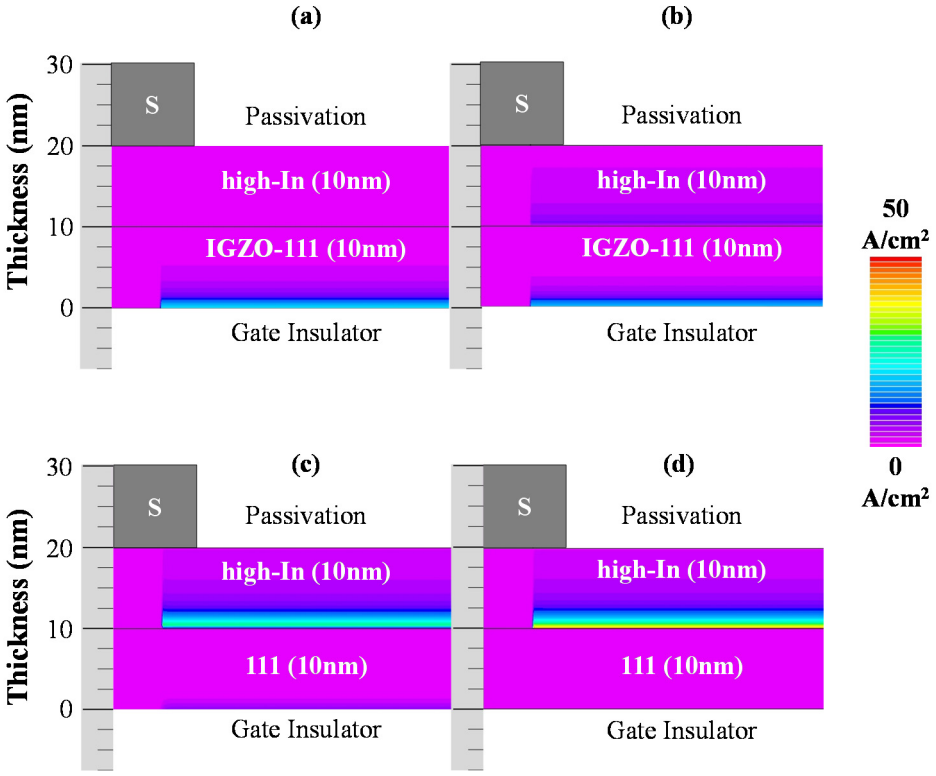

Figure 8. Drain current densities in the hetero-IGZO TFTs with ΔE_c of the (**a**) 0 eV, (**b**) 0.2 eV, (**c**) 0.4 eV, and (**d**) 0.45 eV. The insert is the color coding for the drain current density at V_{GS} = +10 V (V_{DS} = 0.1 V).

4. Conclusions

We investigated the electrical properties of the TFTs with the IGZO heterojunction channels consisting of different compositions. The heterojunction channel was formed to deposit a high-In composition IGZO layer on an IGZO-111 layer. From band alignment analyses, type-II energy band diagram was expected to form at the heterojunction interface with a ΔE_c of ~0.4 eV. In addition, a depth profile of background charge density indicated that a steep ΔE_c was formed at the amorphous IGZO heterojunction interface formed by sputtering. The μ_{FE} of the IGZO TFT with the heterojunction channel improved to 20.1 cm^2 V^{-1} s^{-1}, and its μ_{FE}-V_{GS} curve exhibited a maximum value at applying V_{GS} of ~10 V. The experimental μ_{FE}-V_{GS} curve could be reproduced well by a device simulation when the ΔE_c was assumed at the heterojunction interface. Moreover, the device simulation results indicated that the carrier transport in the hetero-IGZO-TFTs changed from the IGZO-111/GI interface to the heterojunction interface owing to a quantum confinement for electrons when the ΔE_c was formed at the heterojunction interface. Thus, we believe that heterojunction IGZO channel provides an effective method to improve electrical properties of the TFTs.

Supplementary Materials: The following are available online at http://www.mdpi.com/1996-1944/13/8/1935/s1, Figure S1. Changes of transfer characteristics of the (a) homo-IGZO-111, (b) homo-IGZO-high-In, and (c) hetero-IGZO TFTs as a function of PBTS time. The thickness of heterojunction channel is IGZO-high-In/IGZO-111 = 10/10 nm. (d) Relationship between μ_{FE} and ΔV_{th} after the PBTS of 10 ks of the homo- and hetero-IGZO TFTs. The stress temperature was 60 °C and stress gate bias was +20 V, respectively, Figure S2. n_e dependences of measured Hall mobilities (circles) and calculated mobilities (lines) of the IGZO-111 and the IGZO–high-In films.

Author Contributions: Conceptualization, D.K. and M.F.; methodology, D.K., S.H., Y.M. and M.F.; formal analysis, D.K. and S.H.; investigation, D.K. and S.H.; resources; M.F.; date curation; D.K., S.H., Y.M. and M.F.; writing—original draft preparation, D.K. and M.F.; writing—review and editing, D.K. and M.F.; visualization, D.K. and M.F.; supervision, M.F.; project administration, M.F.; funding acquisition, M.F. All authors have read and agreed to the published version of the manuscript.

Funding: Part of this research was funded by the JSPS KAKENHI Grant No.16K06309.

Conflicts of Interest: The authors declare no conflict of interest.

References

1. Nomura, K.; Ohta, H.; Takagi, A.; Kamiya, T.; Hirano, M.; Hosono, H. Room-temperature fabrication of transparent flexible thin-film transistors using amorphous oxide semiconductors. *Nature* **2004**, *432*, 488–492. [CrossRef] [PubMed]
2. Hirao, T.; Furuta, M.; Furuta, H.; Matsuda, T.; Hiramatsu, T.; Hokari, H.; Yoshida, M. 4.1: Distinguished Paper: High Mobility Top-Gate Zinc Oxide Thin-Film Transistors (ZnO-TFTs) for Active-Matrix Liquid Crystal Displays. *SID Symp. Dig. Tech. Pap.* **2006**, *37*, 18. [CrossRef]
3. Jiang, J.; Toda, T.; Hung, M.P.; Wang, D.; Furuta, M. Highly stable fluorine-passivated In–Ga–Zn–O thin-film transistors under positive gate bias and temperature stress. *Appl. Phys. Express* **2014**, *7*, 114103. [CrossRef]
4. Cho, S.H.; Ryu, M.K.; Kim, H.-O.; Kwon, O.S.; Park, E.-S.; Roh, Y.-S.; Hwang, C.-S.; Park, S.-H.K. Influence of gate dielectric/channel interface engineering on the stability of amorphous indium gallium zinc oxide thin-film transistors. *Phys. Status solidi A* **2014**, *211*, 2126–2133. [CrossRef]
5. Wang, D.; Hung, M.P.; Jiang, J.; Toda, T.; Furuta, M. Suppression of Degradation Induced by Negative Gate Bias and Illumination Stress in Amorphous InGaZnO Thin-Film Transistors by Applying Negative Drain Bias. *ACS Appl. Mater. Interfaces* **2014**, *6*, 5713–5718. [CrossRef]
6. Koretomo, D.; Toda, T.; Matsuda, T.; Kimura, M.; Furuta, M. Anomalous Increase in Field-Effect Mobility in In–Ga–Zn–O Thin-Film Transistors Caused by Dry-Etching Damage Through Etch-Stop Layer. *IEEE Trans. Electron Devices* **2016**, *63*, 2785–2789. [CrossRef]
7. Magari, Y.; Makino, H.; Furuta, M. Carrier Generation Mechanism and Origin of Subgap States in Ar- and He-Plasma-Treated In–Ga–Zn–O Thin Films. *ECS J. Solid State Sci. Technol.* **2017**, *6*, Q101–Q107. [CrossRef]
8. Aman, S.G.M.; Magari, Y.; Shimpo, K.; Hirota, Y.; Makino, H.; Koretomo, D.; Furuta, M. Low-temperature (150 °C) activation of Ar + O_2 + H_2-sputtered In–Ga–Zn–O for thin-film transistors. *Appl. Phys. Express* **2018**, *11*, 081101. [CrossRef]
9. Kamiya, T.; Hosono, H. Material characteristics and applications of transparent amorphous oxide semiconductors. *NPG Asia Mater.* **2010**, *2*, 15–22. [CrossRef]
10. Fortunato, E.; Barquinha, P.; Martins, R. Oxide Semiconductor Thin-Film Transistors: A Review of Recent Advances. *Adv. Mater.* **2012**, *24*, 2945–2986. [CrossRef]
11. Raja, J.; Jang, K.; Nguyen, C.P.T.; Yi, J.; Balaji, N.; Hussain, S.Q.; Chatterjee, S. Improvement of Mobility in Oxide-Based Thin Film Transistors: A Brief Review. *Trans. Electr. Electron. Mater.* **2015**, *16*, 234–240. [CrossRef]
12. Liao, C. Mobility impact on compensation performance of AMOLED pixel circuit using IGZO TFTs. *J. Semicond.* **2019**, *40*, 022403. [CrossRef]
13. Arai, T.; Sasaoka, T. 49.1: Invited Paper: Emergent Oxide TFT Technologies for Next-Generation AM-OLED Displays. *SID Symp. Dig. Tech. Pap.* **2011**, *42*, 710–713. [CrossRef]
14. Jang, Y.H.; Kim, D.H.; Choi, W.; Kang, M.-G.; Chun, K.I.; Jeon, J.; Ko, Y.; Choi, U.; Lee, S.-M.; Bae, J.U.; et al. 7-4: Invited Paper: Internal Compensation Type OLED Display Using High Mobility Oxide TFT. *SID Symp. Dig. Tech. Pap.* **2017**, *48*, 76–79. [CrossRef]
15. Nomura, K.; Takagi, A.; Kamiya, T.; Ohta, H.; Hirano, M.; Hosono, H. Amorphous Oxide Semiconductors for High-Performance Flexible Thin-Film Transistors. *Jpn. J. Appl. Phys.* **2006**, *45*, 4303–4308. [CrossRef]
16. Chong, E.; Chun, Y.S.; Lee, S.Y. Amorphous silicon–indium–zinc oxide semiconductor thin film transistors processed below 150 °C. *Appl. Phys. Lett.* **2010**, *97*, 102102. [CrossRef]
17. Kizu, T.; Aikawa, S.; Mitoma, N.; Shimizu, M.; Gao, X.; Lin, M.F.; Nabatame, T.; Tsukagoshi, K. Low-Temperature Processable Amorphous In-WO Thin-Film Transistors with High Mobility and Stability. *Appl. Phys. Lett.* **2014**, *104*, 152103. [CrossRef]
18. Koike, K.; Hama, K.; Nakashima, I.; Takada, G.-Y.; Ozaki, M.; Ogata, K.-I.; Sasa, S.; Inoue, M.; Yano, M. Piezoelectric Carrier Confinement by Lattice Mismatch at ZnO/$Zn_{0.6}Mg_{0.4}O$ Heterointerface. *Jpn. J. Appl. Phys.* **2004**, *43*, L1372–L1375. [CrossRef]
19. Taniguchi, S.; Yokozeki, M.; Ikeda, M.; Suzuki, T.-K. Transparent Oxide Thin-Film Transistors Using n-$(In_2O_3)_{0.9}(SnO_2)_{0.1}$/$InGaZnO_4$ Modulation-Doped Heterostructures. *Jpn. J. Appl. Phys.* **2011**, *50*, 04DF11. [CrossRef]

20. Jeon, S.; Kim, S.I.; Park, S.; Song, I.; Park, J.; Kim, S.; Kim, C. Low-Frequency Noise Performance of a Bilayer InZnO–InGaZnO Thin-Film Transistor for Analog Device Applications. *IEEE Electron Device Lett.* **2010**, *31*, 1128–1130. [CrossRef]
21. Chong, E.; Lee, S.Y. Influence of a highly doped buried layer for HfInZnO thin-film transistors. *Semicond. Sci. Technol.* **2011**, *27*, 12001. [CrossRef]
22. Kim, H.-S.; Park, J.S.; Jeong, H.-K.; Son, K.S.; Kim, T.S.; Seon, J.-B.; Lee, E.; Chung, J.G.; Kim, D.H.; Ryu, M.; et al. Density of States-Based Design of Metal Oxide Thin-Film Transistors for High Mobility and Superior Photostability. *ACS Appl. Mater. Interfaces* **2012**, *4*, 5416–5421. [CrossRef] [PubMed]
23. Jung, H.Y.; Kang, Y.; Hwang, A.Y.; Lee, C.K.; Han, S.; Kim, D.-H.; Bae, J.-U.; Shin, W.-S.; Jeong, J.K. Origin of the improved mobility and photo-bias stability in a double-channel metal oxide transistor. *Sci. Rep.* **2014**, *4*, 3765. [CrossRef]
24. Yang, J.H.; Choi, J.H.; Cho, S.H.; Pi, J.E.; Kim, H.O.; Hwang, C.S.; Park, K.C.; Yoo, S. Highly Stable AlInZnSnO and InZnO Double-Layer Oxide Thin-Film Transistors With Mobility Over 50 $cm^2/V{\cdot}s$ for High-Speed Operation. *IEEE Electron Device Lett.* **2018**, *39*, 508–511. [CrossRef]
25. Park, J.C.; Lee, H.-N. Improvement of the Performance and Stability of Oxide Semiconductor Thin-Film Transistors Using Double-Stacked Active Layers. *IEEE Electron Device Lett.* **2012**, *33*, 818–820. [CrossRef]
26. Saito, N.; Miura, K.; Ueda, T.; Tezuka, T.; Ikeda, K. High-Mobility and H2-Anneal Tolerant InGaSiO/InGaZnO/InGaSiO Double Hetero Channel Thin Film Transistor for Si-LSI Compatible Process. *IEEE J. Electron Devices Soc.* **2018**, *6*, 500–505. [CrossRef]
27. Furuta, M.; Koretomo, D.; Magari, Y.; Aman, S.G.M.; Higashi, R.; Hamada, S.; Hamada, S. Heterojunction channel engineering to enhance performance and reliability of amorphous In–Ga–Zn–O thin-film transistors. *Jpn. J. Appl. Phys.* **2019**, *58*, 090604. [CrossRef]
28. Suko, A.; Jia, J.; Nakamura, S.-I.; Kawashima, E.; Utsuno, F.; Yano, K.; Shigesato, Y. Crystallization behavior of amorphous indium–gallium–zinc-oxide films and its effects on thin-film transistor performance. *Jpn. J. Appl. Phys.* **2016**, *55*, 35504. [CrossRef]
29. Ide, K.; Nomura, K.; Hiramatsu, H.; Kamiya, T.; Hosono, H. Structural relaxation in amorphous oxide semiconductor, a–In–Ga–Zn–O. *J. Appl. Phys.* **2012**, *111*, 073513. [CrossRef]
30. Kim, J.; Bang, J.; Nakamura, N.; Hosono, H. Ultra-wide bandgap amorphous oxide semiconductors for NBIS-free thin-film transistors. *APL Mater.* **2019**, *7*, 022501. [CrossRef]
31. Kim, J.; Hiramatsu, H.; Hosono, H.; Kamiya, T. Effects of sulfur substitution in amorphous InGaZnO4: Optical properties and first-principles calculations. *J. Ceram. Soc. Jpn.* **2015**, *123*, 537–541. [CrossRef]
32. Kim, J.; Miyokawa, N.; Sekiya, T.; Ide, K.; Toda, Y.; Hiramatsu, H.; Hosono, H.; Kamiya, T. Ultrawide band gap amorphous oxide semiconductor, Ga–Zn–O. *Thin Solid Films* **2016**, *614*, 84–89. [CrossRef]
33. Magari, Y.; Hashimoto, S.; Hamada, K.; Furuta, M. Low-Temperature Processed Metal-Semiconductor Field-Effect Transistor with In–Ga–Zn–O/AgOx Schottky Gate. *ECS Trans.* **2016**, *75*, 139–144. [CrossRef]
34. Sze, S.M.; Ng, K.K. *Physics of Semiconductor Devices*, 3rd ed.; Wiley: New York, NY, USA, 2007.
35. Lee, N.H.; Nomura, K.; Kamiya, T.; Hosono, H. Metal-Semiconductor Field-Effect Transistor Made Using Amorphous In-Ga-Zn-O Channel and Bottom Pt Schottky Contact Structure at 200 C. *ECS Solid State Lett.* **2012**, *1*, Q8–Q10. [CrossRef]
36. Kamiya, T.; Hosono, H. (Invited) Roles of Hydrogen in Amorphous Oxide Semiconductor. *ECS Trans.* **2013**, *54*, 103–113. [CrossRef]
37. Jeong, J.; Hong, Y. Debye Length and Active Layer Thickness-Dependent Performance Variations of Amorphous Oxide-Based TFTs. *IEEE Trans. Electron Devices* **2012**, *59*, 710–714. [CrossRef]
38. Abe, K.; Sato, A.; Takahashi, K.; Kumomi, H.; Kamiya, T.; Hosono, H. Mobility- and temperature-dependent device model for amorphous In–Ga–Zn–O thin-film transistors. *Thin Solid Films* **2014**, *559*, 40–43. [CrossRef]
39. Kamiya, T.; Nomura, K.; Hosono, H. Origins of High Mobility and Low Operation Voltage of Amorphous Oxide TFTs: Electronic Structure, Electron Transport, Defects and Doping. *J. Disp. Technol.* **2009**, *5*, 273–288. [CrossRef]

40. Kim, Y.; Bae, M.; Kim, W.; Kong, D.; Jung, H.K.; Kim, H.; Kim, S.; Kim, D.M.; Kim, D.H. Amorphous InGaZnO Thin-Film Transistors—Part I: Complete Extraction of Density of States Over the Full Subband-Gap Energy Range. *IEEE Trans. Electron Devices* **2012**, *59*, 2689–2698. [CrossRef]
41. Kim, S.; Jeon, Y.W.; Kim, Y.; Kong, D.; Jung, H.K.; Bae, M.-K.; Lee, J.-H.; Du Ahn, B.; Park, S.Y.; Park, J.-H.; et al. Impact of Oxygen Flow Rate on the Instability Under Positive Bias Stresses in DC-Sputtered Amorphous InGaZnO Thin-Film Transistors. *IEEE Electron Device Lett.* **2011**, *33*, 62–64. [CrossRef]